JOURNAL OF SPACECRAFT AND ROCKETS
Vol. 38, No. 2, March–April 2001

Experimental Investigation of Reentry Vehicle Aerothermodynamic Problems in Arc-Heated Facilities

A. Gülhan,* B. Esser,† and U. Koch†
DLR, German Aerospace Research Center, 51170 Cologne, Germany

Experimental investigations of local aerothermodynamic phenomena of reentry vehicles in arc-heated facilities are presented. The facility and measurement techniques are described, and performance of the facilities with respect to their reservoir conditions and model surface parameters is presented, as well as the characterization of the hypersonic flowfield by using experimental and numerical tools. Results of different testing activities related to the development of the X-38 vehicle components are discussed. It has been demonstrated that arc-heated facilities are the key tools for the qualification of hot components of reentry vehicles in a realistic aerothermodynamic environment.

Nomenclature

B = magnetic induction, V · s/m^2
$\bar{C}$ = reaction rate constant, kg/(m^{3}s)
F = Lorentz force, N
J = current, A
L = characteristic length, m
p = pressure, hPa
q = heat flux rate, kW/m^2
R = resistance, Ω
r = radius, m
T = temperature, K
t = time, s
V = flow velocity, m/s
θ = angle
ρ = density, kg/m^3

Subscripts

rot = rotational
vib = vibrational
02 = pitot
∞ = freestream

Introduction

DURING the reentry phase of space vehicles into the atmosphere, the nosecap, wing leading edges, and control surfaces are exposed to high thermal loads, which are generated by shock waves heating the air up to temperatures where real-gas effects are important. At these high temperatures, the simulation of reentry aerodynamics requires not only the duplication of Mach number and Reynolds number to consider compressibility and viscous effects, but also matching the real-gas similarity parameters.[1,2]

To distinguish frozen, nonequilibrium and equilibrium flow regimes, characteristic reaction and flow times should be compared. The characteristic flow time is determined by the ratio of a characteristic length L and flow velocity V_∞. The timescale to achieve equilibrium depends on thermal or chemical processes. Whereas three-body collisions are necessary for recombination, binary collisions lead to dissociation. Binary reactions are characterized by the term $\bar{C} \cdot \rho_\infty \cdot L / V_\infty$, where $\bar{C}$ and ρ_∞ are the reaction rate constant and the freestream density. Assuming that $\bar{C}$ is the same as in free flight, the binary scaling factor $\rho_\infty \cdot L$ must be duplicated in addition to the velocity to achieve a true simulation of the dissociation process. This simulation requirement can be satisfied in shock tunnels or other short-time facilities, where due to the high-density level a nearly equilibrium flowfield can be generated, but only for a time duration of a few milliseconds.[3]

The recombination reactions can be enhanced due to catalytic surfaces. The characteristic parameter for this process is the surface Damköhler number, which is defined as the ratio of the characteristic particle diffusion time to the characteristic time for a surface reaction.[4] Long-duration, high-enthalpy tests must be carried out to investigate this phenomenon. Despite restrictions in simulation of flight Reynolds numbers arising from low stagnation pressures, arc-heated wind tunnels are very useful in analyzing the local gas–surface interaction phenomena.

In addition, long-duration, high-enthalpy facilities are one of the key tools in the development and qualification of the hot components of reentry vehicles. A continuous high-enthalpy flowfield can be produced by arc-heated wind tunnels or inductively heated facilities. Whereas so-called plasmatron facilities with an inductive heater are mainly operated in a subsonic flow regime, arc-heated facilities can provide a hypersonic flowfield. The use of these test facilities, particularly in the vehicle design phase, is very important because flight experiments are typically associated with high costs, and numerical simulations contain several shortcomings when analyzing some aerothermodynamic processes such as flow–structure interaction, gap flow, radiation heating, etc. High safety criteria and strong cost and weight reduction aspects of reentry vehicle designs require reliable experimental data from ground-test facilities.

The interpretation of results obtained in ground tests requires a detailed knowledge of the flowfield. In cold facilities, this flow characterization is predominantly done using classical measurement techniques. Because of the severe flow conditions in high-enthalpy facilities, most classical techniques are not applicable, and flow characterization is only possible as a combined effort of classical and sophisticated measurement techniques and numerical tools. All parameters that are not accessible to measurement are characterized by computation; however, even for computation, the high-enthalpy flow environment is severe. Therefore, a combined application of both ground-testing facilities and numerical tools is necessary to cover all physical processes associated with reentry vehicle aerothermodynamics.

This paper summarizes recent activities on local aerothermodynamic problems of reentry vehicles in the arc-heated facilities, Cologne [Lichtbogenbeheizte Anlagen Köln (LBK)]. The necessity of flow characterization and the application of sophisticated nonintrusive measurement techniques in a high-temperature hypersonic flowfield is discussed. The importance of arc-heated facilities in the design of hot structures is demonstrated with different applications from the German program technology for future space transportation systems [Technologien für zukünftige Raumtransportsysteme (TETRA)], which supports the NASA X-38 program.

Received 30 June 2000; revision received 7 November 2000; accepted for publication 8 November 2000. Copyright © 2001 by the authors. Published by the American Institute of Aeronautics and Astronautics, Inc., with permission.

*Research Scientist, Institute of Fluid Mechanics, Wind Tunnel Division Köln-Porz, Linder Höhe. Member AIAA.

†Research Scientist, Institute of Fluid Mechanics, Wind Tunnel Division Köln-Porz, Linder Höhe.

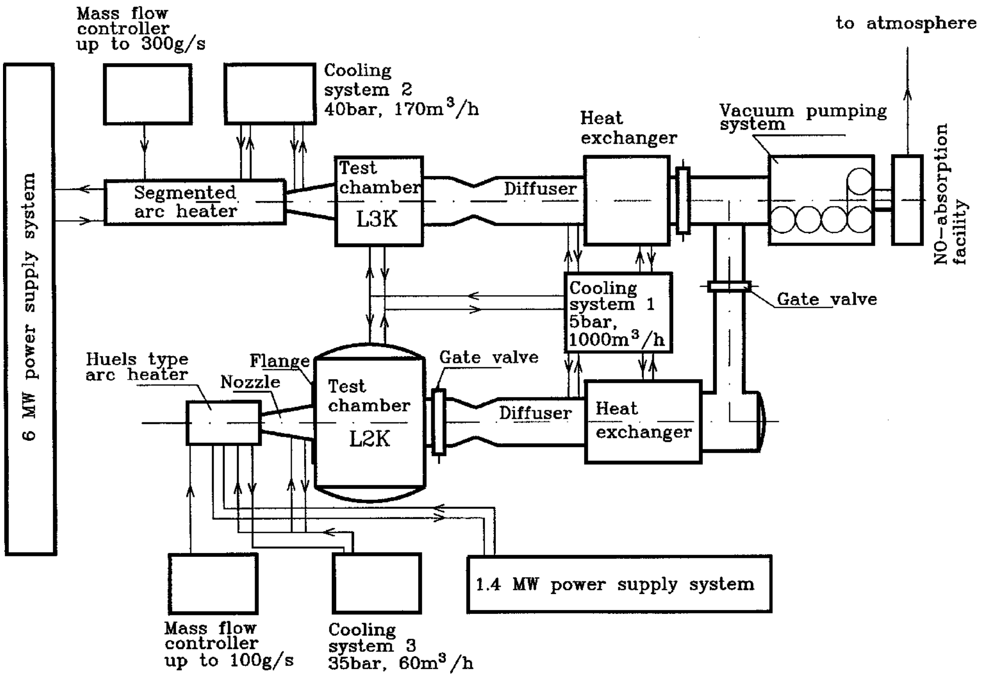

Fig. 1 LBK facility.

Experimental Facility

The LBK arc-heated facility consists of two test legs called L2K and L3K[5] (Fig. 1). Both facilities are connected to a common vacuum pumping system and exhaust-gas cleaning (NO absorption) facility. The vacuum system is composed of five mechanical pumps and allows a pressure below 1 hPa, which is necessary for the ignition of the arc heaters. Three heat exchangers are installed for improved performance. At gas temperatures up to 7000 K, toxic NO_x is formed during operation and is decontaminated in a column by washing the gas with a 10% aqueous NaOH solution before it leaves the facility to the atmosphere. The working gas is supplied from either K-bottles with a volume of 12 m^3 and a pressure of 15 MPa or a 200-m^3 storage tank that can be pressurized up to 6 MPa.

The L2K facility is equipped with a Huels-type arc heater. It consists of two hollow electrodes, placed on the flow axis, which heats the gas supplied from a control system at mass flow rates between 5 and 75 g/s. All heater and nozzle components are cooled with demineralized high-pressure water. Moderate specific enthalpies up to 10 MJ/kg are achieved at a gas mass flow rate of 50 g/s, which corresponds to a reservoir pressure of about 1500 hPa.

The segmented arc heater of L3K consists of three main assemblies: anode, constrictor, and cathode. The constrictor assembly is composed of a converger and a diverger section and the real constrictor, which is made up of 1–6 segment packages, each consisting of 16 identical segments. The performance of the heater can be varied by changing the length of the constrictor. The diameter of the bore is 32 mm. The length-to-diameter ratio L/D of the heater can be varied between 10 and 40. Both anode and cathode assemblies consist of dual electrodes separated by an electrically isolated interelectrode segment. During operation, the arc splits to both electrodes (Fig. 2) so that each electrode is exposed to nearly half of the total current, which reduces the erosion of electrodes. Each electrode is powered by a separate connection including an external adjustable resistor to set current splitting. Current flows over spin coil turns, which are integrated into the electrode assembly circumferentially around the electrode liner, to the liner or vice versa. The Lorentz force induced by the coils' magnetic field forces the arc foot point to rotate on the liner surface. This measure and the tangential injection of argon at the electrodes lead to a further reduction of electrode erosion, i.e., flow contamination. A low flow contamination of less than 40 ppm is achieved even at high arc-heater power levels of about 5 MW. At these low contamination levels, no differences in the heat-flux rates were measured during systematic tests that varied the flow contamination by factor three.

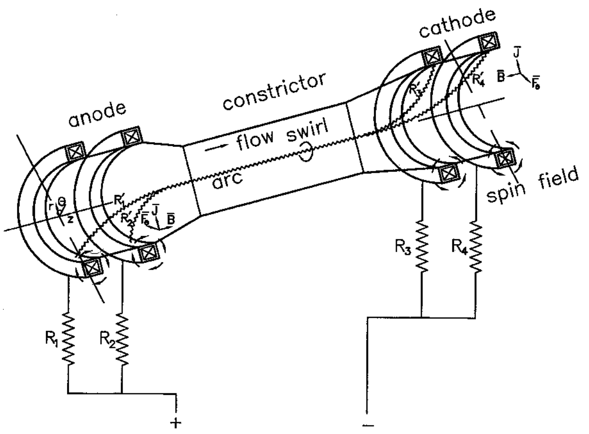

Fig. 2 Schematic view of the L3K segmented arc heater.

The segmented arc heater is operated using air or nitrogen as the working gas. Both gases are supplied by the same control system. For most applications, air is the test gas used. The mass flow rate of air is set with a margin of less than 1.2% of the set point within a range of 30–300 g/s. The mass flow rate transducer operates based on Coriolis force measurement.

A diffuser with a central body is installed downstream of the test chamber. All diffuser parts have double walls and are cooled using low-pressure water. At the diffuser exit, the gas temperature is still beyond 5000 K for some testing conditions. Therefore, a heat exchanger is installed downstream to reduce the gas temperature to below 370 K for all test conditions, which is defined as the upper limit for the operation of the vacuum pumps.

Because individual components of both facilities are exposed to different thermal loads and to satisfy different requirements with respect to their electrical resistivity, two separate water cooling systems are installed: a high-pressure system with demineralized water and a low-pressure system with raw water.

An automatic control system consisting of three programmable control units and a personal computer allows for safe operation. The system allows monitoring of all operational data, as well as adjustment of set point values of interlocks, which depend on the test conditions. The main operation data are recorded by this system. Experimental data are acquired by a separate system with 128 analog inputs, 96 digital input/output channels, and 72 filter and amplifier units, with sampling rates up to 100 kHz.

In both facilities, three different models or probes can be mounted on the model positioning system and be swept into the flowfield, successively. This model positioning system is very convenient for stagnation point tests. A second unit has been designed, to achieve a faster adjustment of angle of attack for the flat-plate test configuration.

Measurement Techniques

Pressure Measurement

During operation, total pressures up to 1.8 MPa are achieved in the arc heaters. Reservoir pressure is measured using pressure gauges with an accuracy of 0.2% of full scale. Because of the acceleration of the high-enthalpy flow through a supersonic nozzle, the freestream static pressure is on the order of a few hectopascal. Therefore, a pressure transducer unit with a range of 10^{-3}–140 hPa is used for the measurement of static pressures. A third transducer is used to measure the pitot pressure. Two measuring heads with a maximum pressure of 100 and 1000 hPa are available. Because of the relatively long test time of arc-heated facilities, moderate response times of the pressure measurements (several seconds) are used for most applications. Considering this aspect and the elimination of the temperature influence on the pressure sensors, all pressure transducers are located outside the test chamber using pressure tubes up to 1.5 m in length.

Surface Temperature Measurement

Different types of thermocouples are used for the measurement of surface temperature. Because of high-temperature effects such as chemical reactions between gaseous particles released from the surface and thermocouple materials, the application of these devices is limited. Another major problem is the stability of adhesives used to fix thermocouples for operation at high temperatures. Therefore, compared to low- or moderate-temperature applications (up to 1400 K), the reliability and accuracy of thermocouple measurements at high surface temperatures is poorer. In the case of a well-defined surface emission factor and transmittance of optical media, nonintrusive measurement techniques such as pyrometry and infrared (IR) thermography provide more reliable data in a high-enthalpy test environment.

To cover the wide temperature range between 300 and 3300 K with a high measurement accuracy of better than ±1%, several spectral pyrometers with complementary measurement ranges are used at LBK.[6] Accurate measurements using spectral pyrometers require reliable data of the model's surface emittance. Because of the emittance's strong dependency on different parameters, for example, wavelength, temperature, etc., the determination of values at high temperatures is a difficult and challenging task. Two two-color pyrometers, which measure the ratio of thermal radiation at two very close wavelengths under the assumption of constant emissivity, are used as complementary systems. With the two-color pyrometers, temperatures between 1073–2273 and 1173–3273 K can be measured. The two-color technique can only be applied for gray surfaces, that is, for a constant emissivity in the spectral range of the pyrometer. Two-color pyrometers can provide uncertain data for optically selective and oxidizing surfaces. An IR camera with a measurement range of 293–2273 K and spectral range of 7.5–12 μm is also available at LBK. It provides 60 frames/s at a 14-bit resolution and has an accuracy of better than ±2% of the full scale.

Several windows are integrated into the test chamber walls. There are two doors with windows of 430 mm diameter in the side walls of the L3K chamber, which allow access to its interior. Two additional optical windows with the same diameter can be installed in the top and bottom wall. Eight further small flanges and two front flanges can be used for optical access or vacuum-tight connections, for example, power supplies for equipment and water hoses or compensation wires for thermocouples. Depending on the test requirements, different pyrometer configurations are used. Figure 3 shows a typical setup of the pyrometers and IR camera for the flat-plate test configuration.

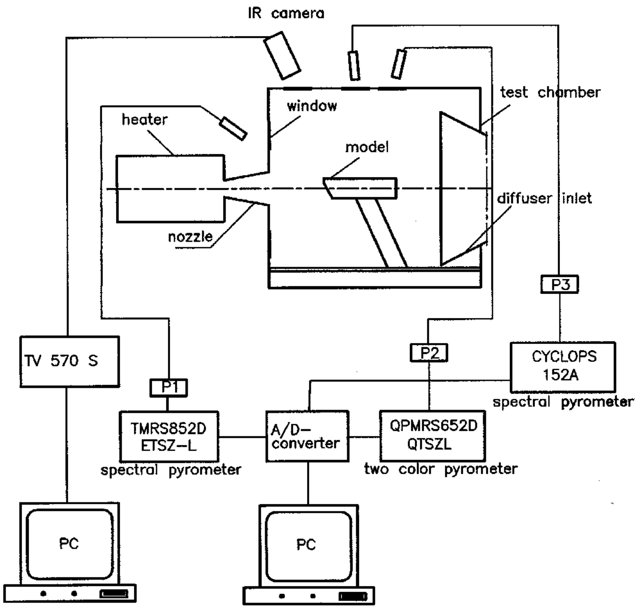

Fig. 3 Pyrometer and IR camera arrangement.

Heat-Flux Measurement

The long available test time of LBK allows thermal protection system (TPS) models to reach radiative equilibrium. When the surface temperature measured with a pyrometer or IR camera is used, the hot-wall heat-flux rate can be determined by application of the Stefan–Boltzmann relation.

For the analysis of aerothermodynamic phenomena, measurement of the cold-wall heat-flux rate plays an important role. Different cold-wall measurement techniques are used. The transient heat-flux probe consists of a copper cylinder with two embedded thermocouples.[7] The probe is surrounded by a thermal insulation to avoid any heat transfer to the holder. Measured temperatures at two locations are used as boundary conditions of a one-dimensional heat conduction in the probe. The heat-flux rate is then determined by solving this parabolic heat transfer equation. The second gauge is based on the calorimeter technique.[8] The front surface of the cylindrical probe, which is exposed to the gas flow, is cooled with water at a known flow rate. An energy balance from the measured flow rate and inlet and outlet water temperatures allows the determination of the steady-state, cold-wall, heat-flux rate. Probes of different materials can be used to investigate the influence of the surface catalysis on the heat transfer. Complementary to these two techniques, Gardon gauges and Vatell heat flux microsensor (HFM) sensors based on the thermopile technique are used for the heat flux measurement.

Spectroscopic Measurement Techniques

The flowfield of both facilities is dominated by thermal and chemical nonequilibrium phenomena. A full understanding of the behaviour of TPS materials in such a flowfield also requires measured data on gas properties. Here again, well-calibrated nonintrusive diagnostic techniques are more reliable tools for the determination of gas properties compared to intrusive techniques, for example, mechanical probes.

Emission and absorption spectroscopy are applied to the measurement of rotational and vibrational temperatures and the concentration of NO molecules. Because these techniques are line-of-sight methods, and the gas properties around the test model may have a heterogeneous distribution, they provide only qualitative results. Accurate local information requires diagnostic techniques with high spatial resolution. To satisfy this requirement, a two-dimensional laser-induced fluorescence (LIF) system is installed. An ArF excimer laser or a dye laser are used as a light source for the excitation of NO molecules or O atoms.[9] The fluorescence spectra are detected by an intensifying charge-coupled device camera with a 384 × 578 pixel array.

Comparative tests were carried out at identical test conditions in L2K using DLR's LIF system and ONERA's coherent anti-Stokes Raman scattering (CARS) system.[10] Table 1 shows a comparison of measured and calculated values of the rotational and vibrational

Table 1 Measured and computed temperatures of NO and N_2 molecules and total density in L2K

Molecule	T_{rot}, K	T_{vib}, K	ρ, kg/m^3
NO (LIF)	300 ± 15	<500	1.7×10^{-4}
N_2 (CARS)	330 ± 10	2510 ± 80	1.4×10^{-4}
CELHYO	305	2690 (N_2)	1.6×10^{-4}

Table 2 Performance of the L2K and L3K facilities

Parameter	L2K	L3K
Nozzle exit diameter, mm	100, 200, 300	100, 200, 300, 400
Mach number	4–8	5–10
Reynolds number, m^{-1}	<104	$<10^5$
Pitot pressure, hPa	5–150	20–350
Total enthalpy, MJ/kg	3–25	6–25
Heat-flux rate, kW/m^2	<2000	<4000
Test duration, s	<7200	<1800

temperatures, T_{rot} and T_{vib}, of NO and N_2 molecules and the total freestream density ρ. The computation was performed with the ONERA CELHYO[10] code including thermal nonequilibrium of O_2 and N_2 molecules. NO molecules are assumed to be in thermal equilibrium. The reservoir pressure and stagnation pressure are 1300 hPa and 3910 K, repectively.

When it is considered that the LIF and CARS techniques use different species (NO and N_2 molecules, respectively) for the spectroscopy, the agreement between experimental and numerical data is good. The data clearly show that in particular N_2 molecules are in thermal nonequilibrium because the vibrational temperature of N_2 is much higher than the rotational temperature.

Performance of LBK

As mentioned before, compared to shock tunnels or hot shot facilities, only low reservoir pressures are achievable in arc-heated facilities. Therefore, the flight Reynolds numbers for the reentry phase of a space vehicle at corresponding Mach numbers cannot be duplicated at standard operation mode of both test legs. Reynolds numbers up to 10^5/m can be achieved. However, the long test time of these facilities and their convenience for the application of sophisticated nonintrusive measurement techniques satisfy the main requirements concerning the investigation of local aerothermodynamic processes such as gap flow, flow separation effects, etc., in a high-temperature environment. Gas parameters behind shock waves in front of TPS components of a reentry vehicle have to be set in ground-testing facilities for the qualification of these components.

In both LBK facilities, hypersonic flow velocities are achieved using conical nozzles with a half-angle of 12 deg. In L2K, nozzle throat diameters of 14, 20, 25, and 29 mm are available. A modular nozzle design with exit diameters of 100, 200, and 300 mm allows Mach numbers between 4 and 8. Stagnation point models with a maximum diameter of 100 mm and flat plates of sizes up to $150 \times 250 \times 50$ mm^3 can be tested in L2K. To keep compatibility with the L2K facility, conical nozzles with the same half-angle of 12 deg are used at L3K. Nozzle throat diameters of 14 and 29 mm are available. The nozzle exit diameter can be set to 100, 200, 300, or 400 mm. In L3K, flat-plate models with main dimensions of $280 \times 350 \times 50$ mm^3 and stagnation point models with a diameter up to 150 mm can be tested in a homogeneous hypersonic flowfield. The main parameters of facility performance are given in Table 2.

Because of its lower power level of 1.4 MW, in L2K specific enthalpies beyond 20 MJ/kg can only be achieved at gas mass flow rates below 10 g/s. The 6-MW power of L3K results in such enthalpies at gas mass flow rates of about 100 g/s. Using the small nozzle throat diameter of 14 mm, higher reservoir pressures up to 1.8 MPa are achieved in the L3K heater.

Flow Characterization

The supersonic high-enthalpy nozzle flow of arc-heated facilities is in nonequilibrium. Therefore, the application of sophisticated measurement techniques and numerical codes at such facilities is essential for a better understanding of the flow. For numerical simulation of the nozzle flow, the CEVCATS-N code[11] of DLR was used. The results are compared to pitot pressure profiles, which were measured in L2K at the test conditions shown in Table 3.

Table 3 Test conditions for pitot pressure measurements in L2K

Condition	L2K/I	L2K/II
Reservoir pressure, hPa	1110 ± 15	1110 ± 15
Reservoir temperature, K	5044 ± 45	5044 ± 45
Total enthalpy, MJ/kg	10.4 ± 0.4	10.4 ± 0.4
Nozzle exit diameter, mm	100	200

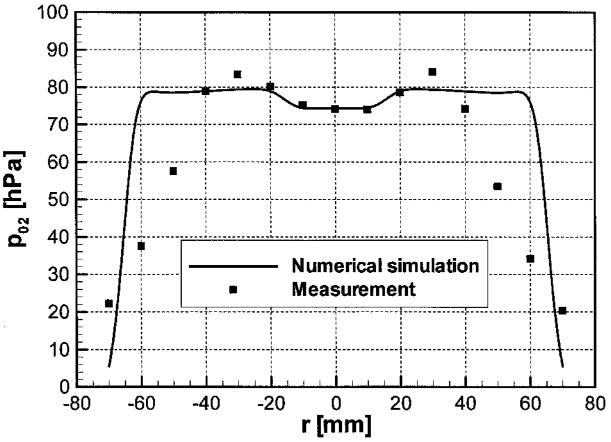

Fig. 4 Comparison of measured and computed pitot pressure profiles 100 mm behind the nozzle exit in L2K (L2K/I condition).

The nozzle throat diameter used for these measurements was 29 mm. Figure 4 shows the measured and computed pitot pressure profiles 100 mm downstream of the 100-mm nozzle exit in L2K. The uncertainty of the measured data is 1.1 hPa. The uncertainties in the reservoir conditions given in Table 3 lead to variations in the computed pitot pressures of ±0.9 hPa.

For the computations, the conical part of the nozzle contour was extended beyond the actual nozzle exit so that the numerical results could easily be compared with measurements taken at different locations. The background pressure is usually lower than the static pressure in the L2K and L3K flowfield, and pressure adaptation is accomplished by an expansion wave. In the numerical simulation configuration, this expansion is neglected. Therefore, systematic deviations between numerical simulation and experiment are to be expected only inside the fan of the expansion wave. Because of the hypersonic flow in the freestream, the fan, which starts at the real nozzle exit position, only slightly approaches the flow axis. Therefore, the unrealistic boundary condition mainly affects a region far from the flow axis. For the case shown in Fig. 4, the measured profile is influenced by the expansion wave only for radii above 40 mm. The slightly wavy profile of the core flow is induced by a compression wave propagating toward the flow axis. This wave is generated in the nozzle throat area at the interface to the conical expansion section.

Pitot pressure profiles 200 mm behind the 200-mm nozzle exit are given in Fig. 5. The slight differences between the numerical and experimental data are probably caused by waves that are generated at the interfaces between the nozzle parts during the experiments. The profile provides a homogenous flow core of approximately 160 mm behind the 200-mm nozzle exit of L2K. At this flow condition the uncertainty of the computed and measured data is ±0.3 and 0.5 hPa, respectively.

The L3K flowfield is characterized for the test conditions shown in Table 4. Figure 6 shows a comparison between measured and computed pitot pressure 654 mm behind the 29 mm nozzle throat, that is, 250 mm downstream of the 200 mm nozzle exit in L3K.[12] The reservoir pressure and stagnation temperature are 4340 hPa and 6000 K, respectively. The agreement between numerical and experimental data is very good. The uncertainties of the computed and measured data are ±0.2 and 0.5 hPa, respectively.

Table 4 Test conditions for pitot pressure measurements in L3K

Condition	L3K/I	L3K/II
Reservoir pressure, hPa	4340 ± 20	6430 ± 35
Reservoir temperature, K	6000 ± 62	6300 ± 68
Total enthalpy, MJ/kg	13.1 ± 0.3	14.1 ± 0.3
Nozzle exit diameter, mm	200	300

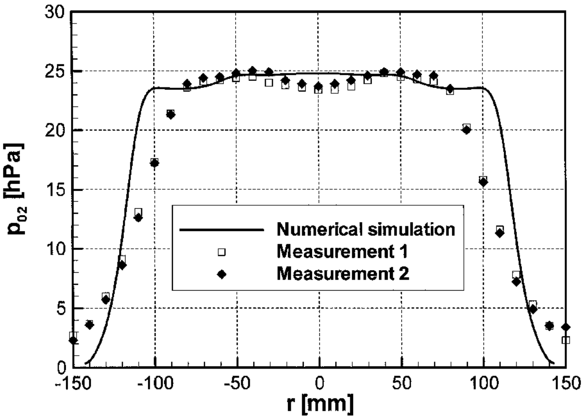

Fig. 5 Comparison of measured and computed pitot pressure profiles 200 mm behind the nozzle exit in L2K (L2K/II condition).

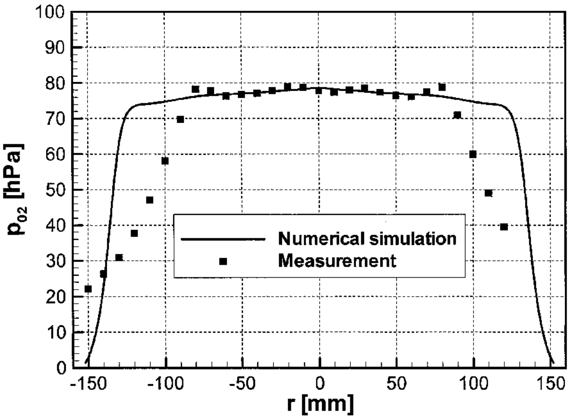

Fig. 6 Comparison of measured and computed pitot pressure profiles 250 mm behind the nozzle exit in L3K (L3K/I condition).

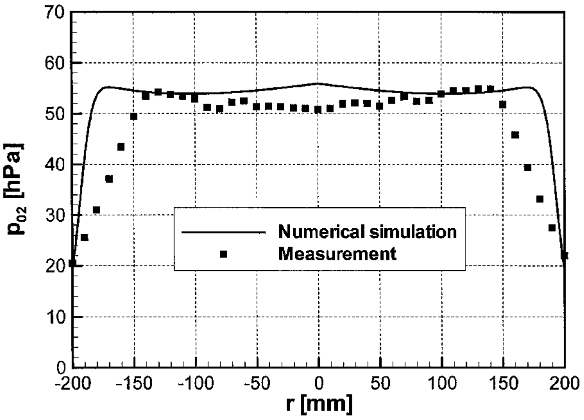

Fig. 7 Comparison of measured and computed pitot pressure profiles 350 mm behind the nozzle exit in L3K (L3K/II condition).

The pitot pressure profiles 350 mm behind the 300-mm nozzle exit at the L3K/II condition are given in Fig. 7. The numerical pitot pressure predictions around the flow axis are higher than the measured data. The reason for this difference is not clear. Near the boundary layer, at radii between 70 and 140 mm, the agreement is good. For this condition, the static pressure at the nozzle exit was almost equivalent to the test chamber's background pressure, and so the numerical results are not significantly affected by the extension of the nozzle contour. The homogeneous flow core behind the nozzle exit diameter of 300 mm is around 280 mm in diameter.

Experiments in LBK

Within the German national space program TETRA, some key components such as the nose cap, nose skirt, and body flaps of the NASA X-38 vehicle have been developed and manufactured. In addition, some flight experiments are foreseen for the first flight of X-38. The L3K facility has been playing a particularly important role in the qualification of these components.

To study the gap heating problem at the hinge line of the control flaps, a flap model with gap components has been tested in L3K[13] (Fig. 8). Tests with the model, which has a constant flap angle of 20 deg, were carried out at angles of attack of 15 and 30 deg. The gap has a constant width of 5 mm. Different gap slots were integrated representing the dynamic seal (Fig. 9).

Because the gap heating is strongly influenced by the flow–structure interaction and radiation, it is very difficult to define similarity parameters for the duplication of flight conditions. The size of the separation bubble is a strong function of the Reynolds number. The gap width of the model is about half of the X-38 hinge line width. The boundary-layer displacement thickness in the gap region of the model is around 40 mm and is much larger (about 300 mm) for the full-scale X-38 vehicle during the reentry phase with high thermal loads at an altitude of 73 km. Therefore, the local Reynolds numbers defined for the boundary-layer edge parameters and the separation bubbles are different for the model and the full-scale vehicle. However, the pressure, temperature, and Mach number distributions in the model boundary-layer flow are very close to those within 40 mm distance from the vehicle surface, and this part of the separated boundary-layer flow has the strongest influence on the gap heating.

The two-dimensional surface temperature distribution measured with an IR camera (Fig. 10) provides very good information about the flowfield and the heat-flux distribution. The surface temperature

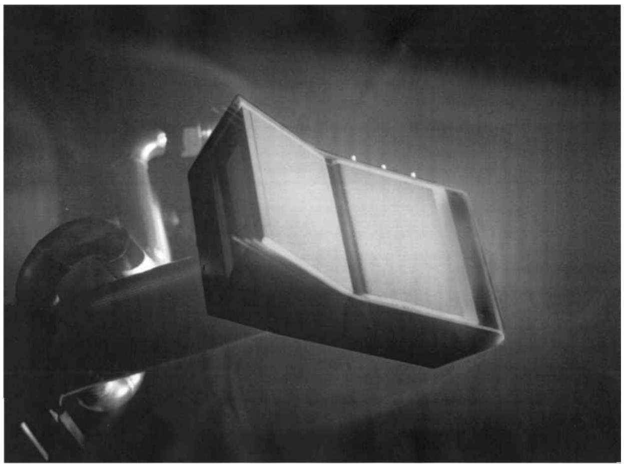

Fig. 8 Flap model in the L3K flowfield.

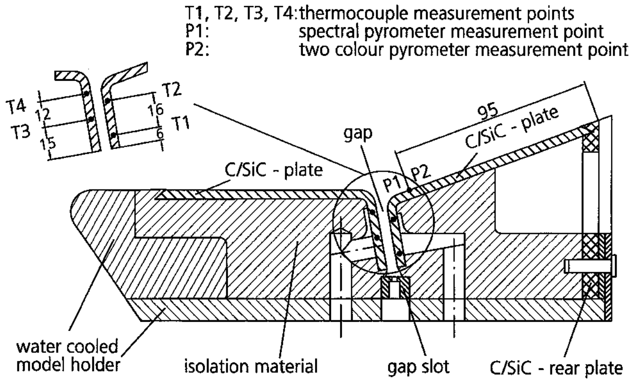

Fig. 9 Cross-sectional view of the flap model.

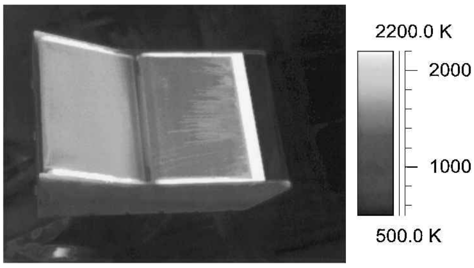

Fig. 10 IR image of the flap model with a closed hinge gap.

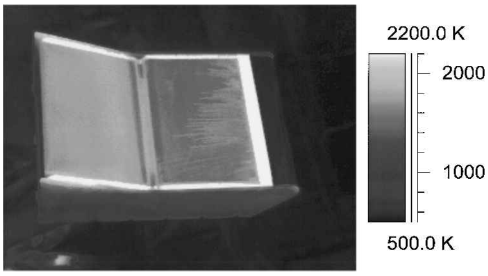

Fig. 11 IR image of the flap model with an open hinge gap.

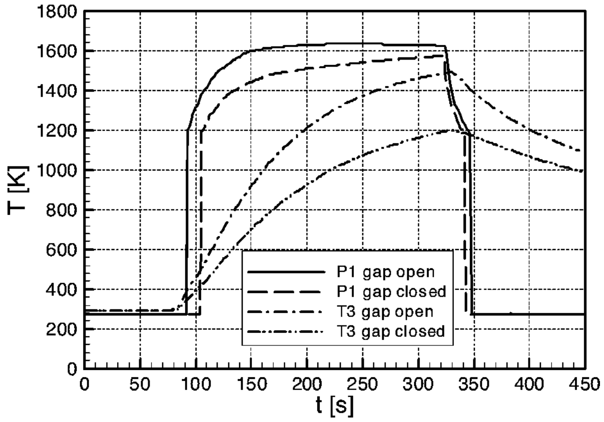

Fig. 12 Histories of surface and gap temperatures.

of the water-cooled model nose is below 800 K. For the isolation material right behind the nose, as well as between the side cover plates and the model, unrealistic high surface temperatures are indicated that relate to two different aspects. First, an emissivity value of 0.8, which is the emissivity of the C/SiC-material, had been used for data reduction, because the C/SiC plates were the main objects of investigation and the data reduction procedure is not able to consider locally different emissivities. It is known that for the wavelength range of 7.5–12 μm the isolation material has a surface emissivity factor of nearly 0.95. Therefore, the real surface temperature of the isolation material is much lower (for about 280 K) than given in Fig. 10. Second is the higher surface catalycity of this material, which leads to higher heat-flux rates, and surface temperatures in a nonequilibrium high-enthalpy flowfield. Although the gap temperature measured with the IR camera must be corrected with respect to the emissivity and view angle, it provides an approximate level of the temperature. The temperature of the closed gap is remarkably lower than the temperature on the ramp.

The IR image of the model with an open gap (Fig. 11) shows that in this case the gap temperature reaches levels that are comparable with the temperatures on the flap. The size of the separation bubble is smaller than that of the model with a closed gap.

In Fig. 12, the history of the flap surface temperature measured with a pyrometer and the development of the gap temperature measured with the thermocouple T3 for open and closed gap configurations is shown. It can be seen that the gap heating in the case of a completely closed gap is a slow process. Opening the gap slot (2 mm width) increases the gap gas flow rate and associated convective heating and causes a faster temperature increase and a higher temperature level in the gap.

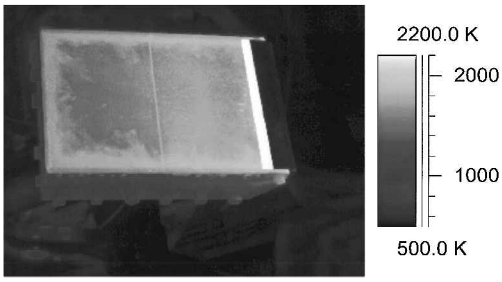

Fig. 13 IR image of the nose cap and nose skirt interface model in L3K.

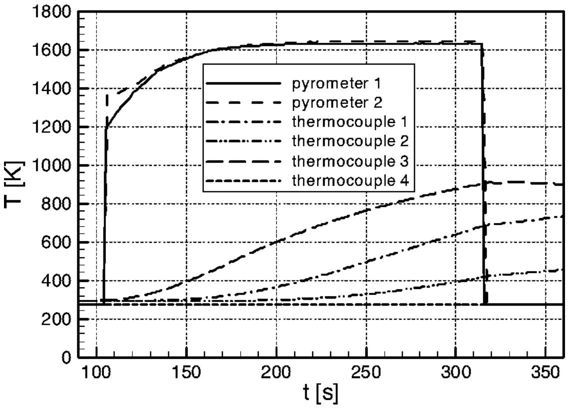

Fig. 14 Measured temperature development on the surface under the high-temperature seal.

Figure 13 shows an IR image of the nose cap and nose skirt interface model with an integrated high-temperature seal. The model was tested in L3K for the verification of the feasibility of the seal concept in the X-38[14] nose cap region. In addition, the temperature development on the surface and under the seal were measured with pyrometers and thermocouples (Fig. 14).

The spectral and two-color pyrometers measured very close temperatures. Under the assumption that the C/C–SiC material behaves as a gray surface at these conditions, the very good agreement of the surface temperatures measured with the two pyrometers indicates the correctness of the emissivity value of 0.85 at a spectral range of around 1 μm. The comparison of these data with the IR data shows that, in the wavelength range of 7.5–12 μm, the surface emissivity of the C/C–SiC material is around 0.8. The data of the spectral and two-color pyrometers were used to determine this emissivity value at the same accuracy as the pyrometer data. Because the material's emissivity is well defined in the spectral range around 1 μm and the transmittance of the optical equipment had been determined using a blackbody source, an accuracy of $\pm 2\%$ could be reached for the pyrometer temperatures. No such systematic study could be performed to determine the accuracy of the thermocouple data. Thermocouples 1 and 2 were installed in the middle of the high-temperature insulation (HTI) part at a depth of 12 and 18 mm from the C/C–SiC plates, respectively. Thermocouples 3 and 4, which are integrated in the same HTI at about 15 mm downstream of the first two thermocouples, have a vertical distance of 15 and 16 mm to the C/C–SiC plate surface. Thermocouple 4 failed before the hot phase of the test. A maximum temperature of about 900 K was measured with the thermocouple 3 after a 240-s test duration, which is remarkably lower than the surface temperature measurement of 1630 K. This fact, the slow decrease of the temperature of thermocouple 3, and the further increase in temperatures of thermocouples 1 and 2 show the dominance of the radiative and conductive heat transfer compared to the convective heating under the flexible gap seal. These observations infer that the flexible seal works quite well, and there is no significant gas flow through the seal at this test condition.

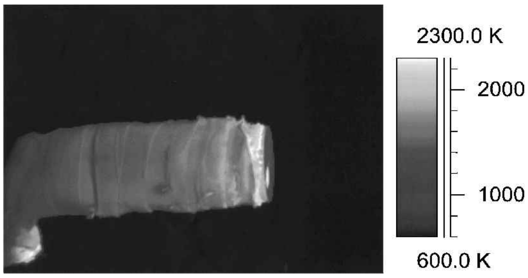

Fig. 15 IR image of the pressure port model.

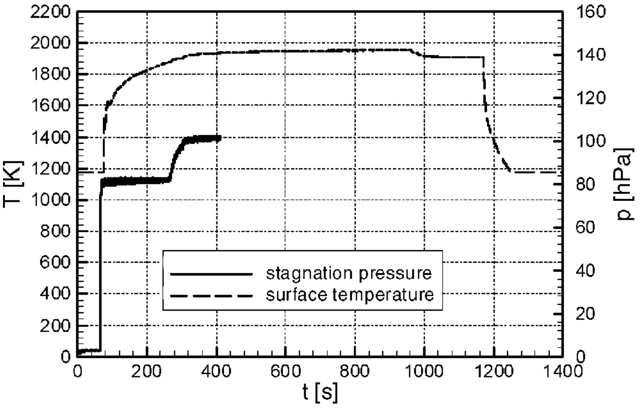

Fig. 16 Surface temperature and stagnation pressure history of the pressure port model in L3K.

DLR will integrate nine pressure ports into the nose cap of the X-38[14] to provide data to the flush air data system for flight control purposes. Because surface temperatures beyond 1900 K are expected for the pressure ports around the stagnation point region, the design of the ports had to be qualified for flight conditions. A stagnation point model with an integrated pressure port and an outer diameter of 70 mm was tested in L3K. To avoid heat transfer through the side wall, the model was coated with an insulation material (Fig. 15). During this test run, a coating with different surface properties compared to the C/C–SiC material of the port was also tested. The IR image of the model shows this coating with a higher surface temperature.

The L3K facility was operated in a dynamic mode, that is, flow conditions were changed during the run to simulate the heat-flux profile of the reentry flight phase of the X-38 (Fig. 16). The stagnation pressure level during the test was higher than the pressure in the early phase of the reentry.

The model was injected into the flow at a relatively low flow energy level. This low energy and the thermal capacity of the model assembly avoided high-temperature gradients in the structure. In this early phase, the pressure port measures a stagnation pressure of about 80 hPa. After 300 s, the flow rate and the arc current were increased to their final levels. The test duration at the steady-state test condition with a stagnation pressure of 101 hPa and surface temperature of 1945 K was 670 s. Then the flow energy was decreased to the level before the steady-state phase. Although the stagnation pressure reached the same level around 80 hPa, the surface temperature was higher than the initial temperature. After 300-s testing at this final condition, the model was removed from the flow. Inspection of the pressure port after the test showed no anomalies and confirmed a stable behavior of the port during the test.

The aerothermodynamic measurement system (AMS), which consists of a heat-flux sensor, two surface temperature sensors, and a pressure port, was qualified in L2K (Fig. 17) for the first X-38 flight experiment.[15,16] The heat-flux sensor consists of a heat-flux probe of thermopile type (HFS) and a resistance thermoelement (RTS) deposited on the surface. The surface temperature measurement is used for the correction of the measured heat-flux rate depending on the wall temperature. The sensor enables measurement of heat-flux rates up to 1150 $\mathrm{kW/m^2}$ with a very short response time of 6 μs. It can be used up to a maximum surface temperature of 1132 K. The instrumented sensor plug (ISP) integrated in a flexible external insulation (FEI) blanket was installed in a water-cooled model holder of L2K with an insulation layer at the interfaces. Complementary measurements of the surface temperature development on the ISP and FEI with pyrometers and an IR camera provided very useful data concerning the thermal response of the total system.

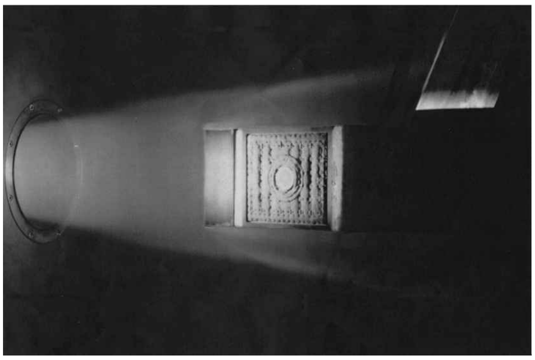

Fig. 17 AMS in the hypersonic flowfield of L2K.

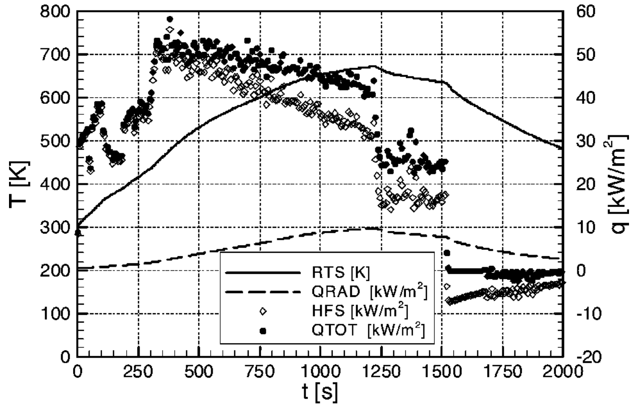

Fig. 18 Temperature and heat-flux history during test of AMS unit in L2K.

To simulate the variable aerothermal loads of the reentry trajectory, the L2K facility was also operated in a dynamic mode. The model was injected into the L2K flowfield at a low-energy level, 500 mm behind the 200-mm nozzle exit. Then, parallel to an increase of the gas mass flow rate and the arc current, the model was moved axially toward the nozzle exit, increasing surface pressure and heat flux. After 320 s, the steady-state flow condition was maintained, and the model was at the final measurement location of 300 mm. Because the homogeneous flow core is larger than the model size at all model locations, the movement of the model has almost no impact on the lateral distribution of the model surface parameters.

The history of the sensor data during the test is given in Fig. 18. The model surface temperature (RTS) increased continuously and caused a decrease in the heat-flux rate (HFS) measured with the sensor. The radiative heat loss QRAD was calculated from the surface temperature data using the Stefan–Boltzmann relation. The total heat-flux rate QTOT is the sum of the HFS and QRAD. After 1200 s, the model was moved back to 500 mm, and the flow energy density was reduced. Finally, the model was moved out of the flow and the hot test phase was terminated at 1518 s. The test chamber pressurization began after around 1680 s. The start of this phase can be seen on the signal of the HFS sensor, whose high sensitivity detects weak convection inside the test chamber.

Conclusions

Based on the experience gained through involvement in former European space activities like Hermes and Manned Space

Transportation Program (MSTP), and due to their improved facility performance, both DLR arc-heated facilities L2K and L3K have been used for the development of several TPS components of the X-38 vehicle. Because of the high costs of flight experiments and the shortcomings of numerical tools with respect to local aerothermodynamic processes, the use of the long-duration, high-enthalpy facilities continues to be very important, particularly during the design phase of a reentry vehicle. Available technologies do not allow the development of a ground-testing facility in the near future that allows the qualification of thermally critical components of a full-scale vehicle at reentry conditions. Therefore, arc-heated facilities such as L2K and L3K will remain important tools for the development and qualification of hot structure elements and flight sensors with reasonable associated costs. The application of sophisticated measurement techniques, such as LIF for the determination of the flow parameters combined with modern IR devices used to measure the surface temperature, provides useful data for the validation of numerical tools.

Acknowledgments

The test activities on X-38 components in L2K and L3K have been performed with the financial support of the German national technology program for future space transport vehicles, Technologien für zukünftige Raumtransportsysteme (TETRA). The companies MAN-Technologie and OHB, and the DLR, Institute for Structure and Design are gratefully acknowledged for providing the models and materials.

References

[1] Dorrance, W. H., *Viscous Hypersonic Flow*, McGraw–Hill, New York, 1962, pp. 69–101.

[2] Koppenwallner, G., "Low Density Facilities," Third Europe/U.S. Short Course in Hypersonics, Aachen Technical Univ. (RWTH), Aachen, Germany, 1990.

[3] Esser, B., Grönig, H., and Olivier, H., "High-Enthalpy Testing in Hypersonic Shock Tunnels," *Advance in Hypersonics*, edited by J. J. Bertin, J. Periaux, and J. Ballmann, Vol. 1, Birkhäuser, Boston, 1992, pp. 182–258.

[4] Kindler, K., "Aerodynamic Simulation Conditions in Arc Heated Wind Tunnels," *Proceedings of the 2nd European Aerospace Conference in Space Transportation*, SP-293, ESA, May 1989.

[5] Gülhan, A., "Arc Heated Facility LBK as a Tool to Study High Temperature Phenomena at Reentry Conditions," DLR, German Aerospace Research Center, Rept. IB-39113-97A05, Cologne, Germany, Oct. 1997.

[6] Gülhan, A., "Application of Pyrometry and IR Thermography to High Surface Temperature Measurements," RTO/von Kármán Inst. Special Course on Measurement Techniques for High Enthalpy and Plasma Flows, Rept. RTO-EN-8, RTO/NATO, Oct. 1999.

[7] Kindler, K., "Ermittlung einer zeitlich veränderlichen Wärmebelastung auf einen endlichen Zylinder," *5.* Jahrestagung der DGLR, Vortrag Nr. 72, Berlin, 1972.

[8] Gülhan, A., "Heat Flux Measurements in High Enthalpy Flows," RTO/von Kármán Inst. Special Course on Measurement Techniques for High Enthalpy and Plasma Flows, Rept. RTO-EN-8, RTO/NATO, Oct. 1999.

[9] Koch, U., Gülhan, A., Esser, B., Grisch, F., and Bouchardy, P., "Rotational and Vibrational Temperature and Density Measurements by Planar Laser Induced NO-Fluorescence Spectroscopy in a Nonequilibrium High Enthalpy Flow," AGARD Conf. on Advanced Aerodynamic Measurement Technology, CP-601, AGARD, 1997, Paper 15.

[10] Grisch, F., Bouchardy, P., Joly, V., Koch, U., and Gülhan, A., "Coherent Anti-Stokes Raman Scattering Measurements and Computational Modelling of Nonequilibrium Flow," *AIAA Journal*, Vol. 38, No. 9, 2000, pp. 1669–1675.

[11] Brück, S., and Radespiel, R., "Extension of the Euler/Navier–Stokes Code CEVCATS to Viscous Nonequilibrium Flows," DLR, German Aerospace Research Center, Rept. DLR-IB 223-95A64, Göttingen, Germany, May 1996.

[12] Esser, B., and Gülhan, A., "Flow Field Characterisation of DLR's Arc Heated Facilities L2K and L3K," *Proceedings of the 3rd European Symposium on Aerothermodynamics for Space Vehicles*, ESTEC, SP-426, European Space Research and Technology Centre, Noordwijk, The Netherlands, 1998.

[13] Gülhan, A., Esser, B., and Koch, U., "Experimental Investigation of Gap Flows on a Flap Model in the Arc Heated Facility L3K," DLR, German Aerospace Research Center, Rept. DLR IB-39113-99C01, Cologne, Germany, Sept. 1999.

[14] Hald, H., Weihs, H., et al., "Development of a CMC Nose Cap System for X-38," International Symposium on Atmospheric Reentry Vehicles and Systems, Archachon, France, March 1999.

[15] Janovsky, R., Romberg, O., and Tausche, M., "A Contribution to the Aerothermodynamic Measurement System of the X-38," International Symposium on Atmospheric Reentry Vehicles and Systems, Archachon, France, March 1999.

[16] Janovsky, R., Romberg, O., Tausche, M., and Wienss, W., "The Aerothermodynamic Measurement System of the X-38," AIAA International Space Planes and Hypersonic Systems and Technology Conf., Nov. 1999.

M. Torres
Associate Editor